Deep Learning-Based Speed Limit Sign Detection Using YOLOv11 Applied to Speed Regulation in Electric Vehicles for ADAS

Mohammed Chaman
Laboratory of Electronic Systems Information Processing Mechanics and Energetics, Ibn Tofail University, Kenitra, Morocco
mohammed.chaman@uit.ac.ma (corresponding author)

Anas El Maliki
Laboratory of Electronic Systems Information Processing Mechanics and Energetics, Ibn Tofail University, Kenitra, Morocco
anas.elmaliki@uit.ac.ma

Hamad Dahou
Laboratory of Electronic Systems Information Processing Mechanics and Energetics, Ibn Tofail University, Kenitra, Morocco
hamad.dahou@gmail.com

Rachid El Gouri
Laboratory of Advanced Systems Engineering, Ibn Tofail University, Kenitra, Morocco
elgouri.rachid@yahoo.fr

Hlou Laamari
Laboratory of Electronic Systems Information Processing Mechanics and Energetics, Ibn Tofail University, Kenitra, Morocco
hloul@yahoo.com

Abdelkader Hadjoudja
Laboratory of Electronic Systems Information Processing Mechanics and Energetics, Ibn Tofail University, Kenitra, Morocco
abdelkader.hadjoudja@uit.ac.ma

Received: 8 April 2025 | Revised: 1 May 2025 and 6 May 2025 | Accepted: 10 May 2025

 DOI: https://doi.org/10.48084/etasr.11320

ABSTRACT

This study presents an effective speed limit sign detection and automatic speed regulation system using YOLOv11 within an Advanced Driver Assistance System (ADAS) framework. By integrating rapid sign detection with vector control of Permanent Magnet Synchronous Motors (PMSM), the proposed system delivers real-time speed limit compliance and improved vehicle performance. The YOLOv11 model was trained on a dataset of 23,000 traffic sign images. Experimental results demonstrate high performance, with a mean Average Precision (mAP) of 99.6% (mAP@50) and 86.2% (mAP@50–95), alongside 99.2% precision and 98.5% recall, underscoring the model's effectiveness. This work concludes that combining deep learning–based traffic sign recognition with advanced motor control significantly enhances ADAS capabilities and paves the way for future research into integrated, high-accuracy solutions for sustainable transportation.

Keywords-YOLOv11; speed limit sign detection; Advanced Driver Assistance Systems (ADAS); electric vehicles; speed regulation; deep learning

I. INTRODUCTION

Ensuring road safety and reducing traffic accidents remain central objectives in the development of autonomous driving technologies and Advanced Driver Assistance Systems (ADAS) [1]. Among various factors contributing to safe transportation, speed limit signs are crucial, as they regulate traffic flow, enforce legal speed constraints, and promote responsible driving. Over the past decade, significant advancements in computer vision and deep learning have revolutionized traffic sign detection systems [2]. Despite such progress, several challenges persist. Traditional detection methods often fail under realistic scenarios, particularly when speed limit signs are partially obscured, damaged, or dirty. Additional complications arise from varying lighting, adverse weather, and the diversity of traffic sign designs across countries, all of which hinder consistent and accurate detection [3]. For Electric Vehicles (EVs), accurate speed limit detection holds special significance due to their reliance on Permanent Magnet Synchronous Motors (PMSMs), chosen for their high-power density and rapid dynamic response. Utilizing detected speed limits to dynamically adjust PMSM parameters allows effective management of torque and energy consumption, thereby optimizing vehicle performance and efficiency. Consequently, precise detection directly contributes to improved vehicle control, energy management, regulatory compliance, and enhanced sustainability in transportation [3, 4].

Deep learning has substantially improved object detection methods, especially in traffic sign recognition. Two-Stage detectors, including Region-based Convolutional Neural Networks (R-CNN), Spatial Pyramid Pooling (SPP)-Net, fast R-CNN, faster R-CNN, and mask R-CNN, achieve high accuracy but are computationally intensive, making them unsuitable for real-time applications in embedded vehicle systems [5]. In contrast, one-stage detectors like Single Shot Detector (SSD) and You Only Look Once (YOLO) unify region proposal and classification into a single pipeline, enabling faster inference and lower computational load, key advantages for onboard ADAS deployment [6]. Nonetheless, detecting small, partially occluded speed limit signs remains challenging. Previous YOLO versions, like YOLOv8, have reported strong results (mAP@50 of 99.1% and mAP@50:95 of 83.5%) [7]. YOLOv11 represents a significant advancement, offering enhanced computational efficiency and real-time capability, both critical for in-vehicle systems [8]. It incorporates architectural innovations, including the C3k2 block, SPPF, and Cross-Scale Pixel Spatial Attention (C2PSA) modules, which improve detection precision, recall, and inference speed [9]. Comparative analyses affirm YOLOv11's superiority in detecting small objects swiftly and accurately, even in complex real-world scenarios, making it well-suited for ADAS applications with limited processing resources.

In parallel, advanced PMSM control strategies, including vector control, Sliding Mode Control (SMC), Direct Torque Control (DTC), and Flux Weakening Control (FWC), facilitate precise real-time torque and speed management [10-12]. By integrating YOLOv11-based detection with PMSM control, vehicles can dynamically adapt to posted speed limits while optimizing energy consumption.

In this study, we propose an integrated approach that combines precise speed limit sign detection using YOLOv11 with vector control of PMSM to enhance both road safety and EV efficiency [13]. This integration enables high detection accuracy, real-time responsiveness, reduced computational overhead, and significant improvements in vehicle safety, energy efficiency, and regulatory compliance.

II. METHODOLOGY

A. *YOLOv11 Model for Speed Limit Sign Detection*

YOLOv11 marks a significant advancement within the Ultralytics YOLO series, achieving an optimal balance between detection accuracy, inference speed, and computational efficiency, features that make it particularly well-suited for real-time ADAS applications. As the latest evolution in the YOLO family, YOLOv11 introduces key architectural innovations designed to enhance feature representation while enabling efficient deployment on embedded automotive platforms [8, 14]. Structurally, YOLOv11 replaces the earlier C2f module with the C3k2 module, utilizing a multibranch architecture combined with residual connections to improve multiscale feature extraction. This approach maintains a lightweight structure while significantly enhancing feature adaptability. Additionally, YOLOv11 integrates the Spatial Pyramid Pooling Fast (SPPF) module, which effectively aggregates multiscale contextual information through sequential MaxPooling operations, capturing rich local and global semantics without increasing computational overhead. Another significant enhancement is the C2PSA module, positioned after the SPPF block. This module leverages pixel-level spatial attention mechanisms to refine feature maps, focusing on critical regions and boosting detection performance in complex scenes with multiple objects or occlusions.

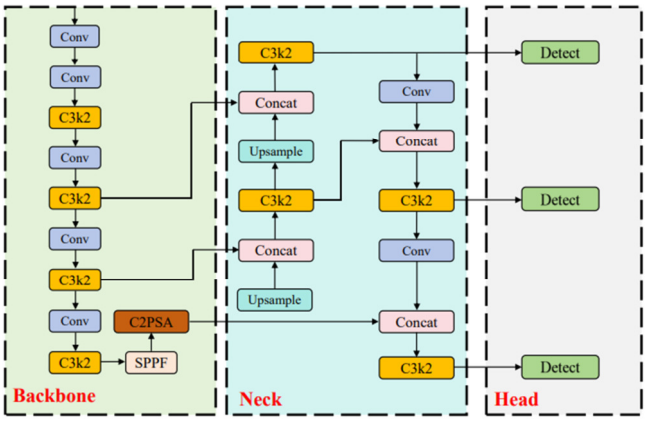

Fig. 1. Overall architecture of YOLOv11 network.

As illustrated in Figure 1, the overall YOLOv11 architecture comprises three main components: the Backbone, Neck, and Head. The Backbone employs convolutional layers, C3k2 blocks, and attention modules (SPPF, C2PSA) to extract

deep, multiscale features. The Neck module integrates these features across different resolutions through upsampling, concatenation, and additional C3k2 blocks, ensuring robust fusion and semantic preservation. Finally, the Head module performs precise bounding-box regression and object classification at multiple scales. Moreover, the adoption of depth-wise separable convolutions in the detection head significantly reduces computational redundancy, enhancing throughput and further optimizing real-time operation

B. Performance Metrics

To evaluate the performance of the speed limit sign detection algorithm under real-time operational constraints, four primary metrics were employed [15]: precision, recall, Average Precision (AP), mean Average Precision (mAP), and F1-score. Precision measures the proportion of correctly predicted positive instances out of all predicted positives, while recall quantifies the proportion of correctly predicted positives among all actual positives. AP is defined as the area under the precision-recall curve for a single class, and mAP is the average of AP scores across all classes, providing a comprehensive measure of overall detection performance. The F1-score measures the harmonic mean of precision and recall, making it a particularly effective metric for evaluating model performance on imbalanced datasets or when classifying minority classes. These metrics are formally defined as follows, where TP denotes true positives, FP false positives, and FN false negatives:

$$\text{Precision} = \frac{\text{TP}}{\text{TP+FP}} \cdot 100\% \quad (1)$$

$$\text{Recall} = \frac{\text{TP}}{\text{TP+FN}} \cdot 100\% \quad (2)$$

$$\text{AP} = \int_0^1 P(R)\text{d}R \quad (3)$$

$$\text{mAP} = \frac{1}{C}\sum_{j=1}^{c} (AP)j \quad (4)$$

$$\text{F1} - \text{score} = 2\frac{\text{Precision} \cdot \text{Recall}}{\text{Precision+Recall}} \cdot 100\% \quad (5)$$

where C represents the total number of classes, and AP_i is the AP for the i^{th} class.

C. Electric Vehicle (EV) Description

An EV uses electric motors for propulsion, replacing traditional internal combustion engines. Figure 2 illustrates the key components of the EV drivetrain, which are fundamental for understanding the propulsion system. Specifically, the drivetrain consists of: 1) a converter/inverter that transforms Direct Current (DC) energy from the battery into Alternating Current (AC) to drive the motor, 2) a PMSM that generates mechanical torque, 3) a mechanical transmission that adapts motor torque and speed to the wheels, and 4) the wheels themselves, which transmit the motion to the road surface [4, 16].

The motor produces torque by converting electrical energy into mechanical energy, which propels the vehicle. The vehicle speed V is related to the motor's rotational speed ω_r through (6):

$$V = k\omega_r \quad (6)$$

where k is the transmission ratio. On dry road surfaces, where wheel slip is negligible, the relationship between vehicle speed V and wheel angular speed ω is given by:

$$V = R\omega \quad (7)$$

where R is the wheel radius.

The voltage-fed PMSM can be modeled by the following dynamic equations in the d–q rotating reference frame:

$$V_d = RI_d + L_d\frac{dI_d}{dt} - \omega L_q I_q \quad (8)$$

$$V_q = RI_q + L_q\frac{dI_q}{dt} + \omega\left(L_d I_d + \varphi_f\right) \quad (9)$$

$$\frac{dI_d}{dt} = \frac{V_d}{L_d} - \frac{RI_d}{L_d} + \frac{\omega L_q I_q}{L_d} \quad (10)$$

$$\frac{dI_q}{dt} = \frac{V_q}{L_q} - \frac{RI_q}{L_q} - \frac{\omega L_d I_d}{L_q} - \frac{\omega\varphi_f}{L_q} \quad (11)$$

$$\frac{d\omega}{dt} = \frac{1}{J}(C_e - C_r - f\omega) \quad (12)$$

$$C_e = \frac{3}{2}P\left(\left(L_d - L_q\right)I_d I_q + \varphi_f I_q\right) \quad (13)$$

where V_q and V_d represent the d-q axis voltages, while I_d and I_q are the corresponding d-q axis currents. L_d and L_q denote the d-q axis inductances, and φ_f is the permanent magnet flux linking the stator. J is the combined moment of inertia of the motor and load, C_e is the electromagnetic torque produced by the motor, and C_r is the resistive load torque opposing motion. Additionally, f is the viscous friction coefficient accounting for mechanical losses, and P is the number of pole pairs of the PMSM.

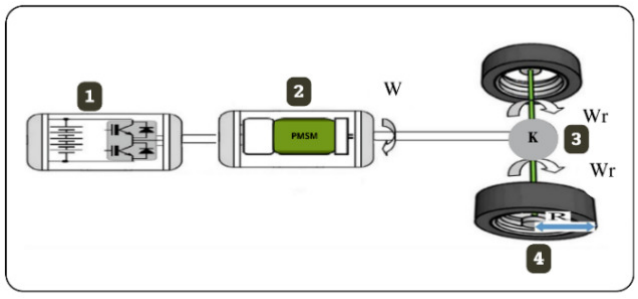

Fig. 2. EV drivetrain architecture: 1) converter/inverter, 2) PMSM motor, 3) transmission (gearbox), 4) wheels.

D. Speed Regulation of PMSM by Vector Control

Initially, a PMSM model is formulated using a state-space approach that integrates the electrical, magnetic, and mechanical dynamics described by equations (10)-(13). A vector control strategy is then applied to achieve precise and efficient motor speed regulation. This approach utilizes a Proportional-Integral (PI) controller, electromechanical decoupling, state feedback, and specific reference equations for torque C_e^*, current I_{qref}, and voltages V_{qref} and V_{dref}. The system inputs include the measured motor speed V_m and a reference speed V, derived from external sources such as detected speed limit signs. The outputs are direct and

quadrature axis voltages V_d and V_q, defined in (8) and (9), respectively. The central Control Block compares the measured motor speed V_m with the reference speed V, generating appropriate voltage references (V_{dref}, V_{qref}) in real-time. This enables optimal control of motor speed and torque while maintaining system stability, safety, and efficiency. Through the PI controller and closed-loop feedback, the system dynamically corrects deviations between actual and desired motor behavior

As depicted in Figure 3, the control architecture incorporates the inverse Park transformation to convert the reference voltages (V_{dref}, V_{qref}) into three-phase voltages V_a, V_b, V_c. These voltages pass through an inverter using a transition matrix T. The resulting three-phase voltages and currents are then transformed back into the d–q reference frame using the Park transformation, yielding the actual axis voltages V_d, V_q. This decoupling mechanism allows for independent control of flux and torque, thereby enhancing dynamic performance. The control system is governed by the following reference equations:

$$I_{qref} = C_e^* \left(\frac{2}{3P\varphi_f^*}\right) \quad (14)$$

$$V_{dref} = -\omega^* L_q I_{qref} \quad (15)$$

$$V_{qref} = RI_{qref} + \omega\varphi_f^* \quad (16)$$

where I_{qref} is the reference quadrature-axis current, C_e^* is the reference electromagnetic torque, ω^* is the reference angular speed, and φ_f^* denotes the reference permanent magnet flux.

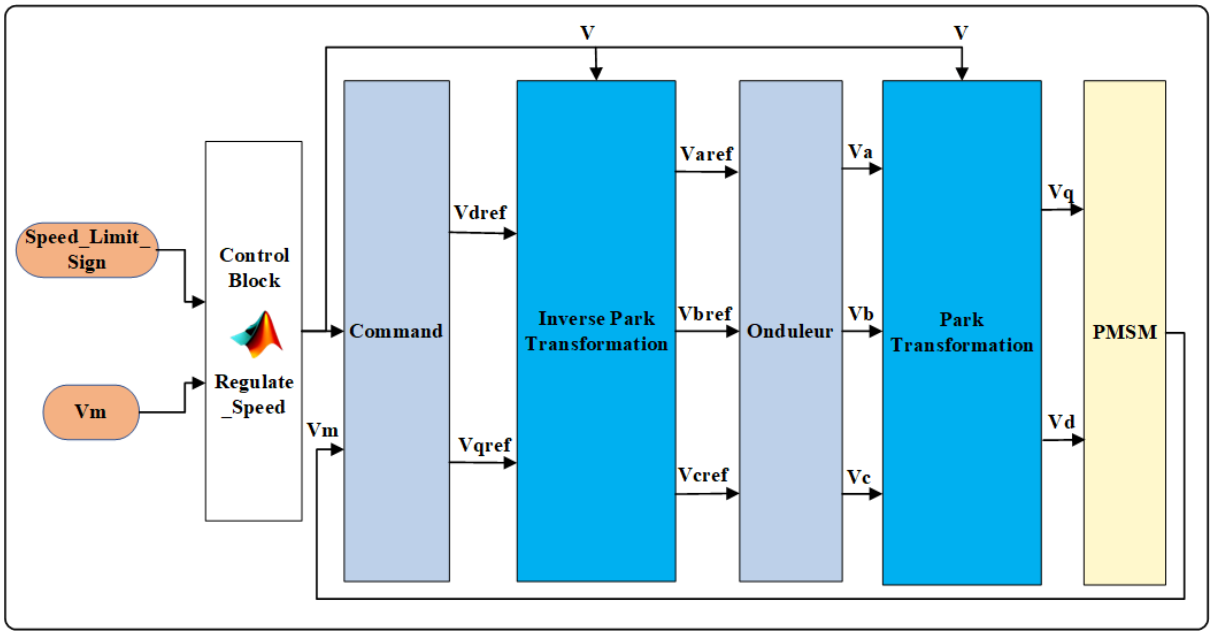

Fig. 3. Vector control architecture for speed regulation.

E. Case Study of Proposed Method

The speed limit sign perception system developed in this study incorporates a high-resolution camera mounted behind the vehicle's interior rearview mirror. This strategic placement enables continuous, real-time image acquisition, significantly enhancing the system's ability to detect various traffic signs under diverse environmental conditions.

To train the detection model, a custom dataset of 23,000 manually labeled images was constructed, comprising 10 speed limit classes ranging from 20 to 120 km/h, covering commonly observed regulatory signs. Table I summarizes the image distribution across the speed limit classes used in the training process. Each image was annotated using Roboflow and exported in YOLO format to ensure compatibility with the training pipeline. All images were resized to 640 × 640 pixels to strike a balance between visual clarity and computational efficiency. To enhance model robustness and mitigate overfitting, various data augmentation techniques were applied, including flipping, rotation, noise addition, and exposure adjustments. The dataset was divided into 70% for training, 20% for validation, and 10% for testing, as shown in Figure 4.

TABLE I. DISTRIBUTION OF IMAGES PER SPEED LIMIT CLASS IN THE CONSTRUCTED DATASET

Speed Limit (km/h)	Number of Images
20	1256
30	3120
40	3253
50	1437
60	3015
70	3065
80	1425
90	1563
100	2710
120	2156

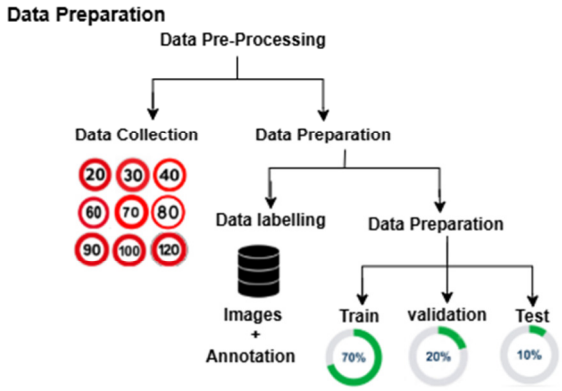

Fig. 4. Dataset preparation workflow.

To assess generalization performance, complex urban environments were selected from cities such as Casablanca, Kenitra, Tangier, Ksar Sghir, Meknes, and Khemisset. These scenarios introduced challenges like partially obscured and weather-damaged signs, closely simulating real-world driving conditions. Figure 5 presents examples of these challenging environments, enabling rigorous evaluation of the model's detection capabilities. The speed control system was simulated using a numerical approach, with the PMSM directly powered by a 220/380 V supply on a balanced three-phase grid operating at a fixed frequency of 50 Hz. The simulation was implemented in MATLAB/Simulink, with machine parameters detailed in Table II. This setup enabled precise modeling of the PMSM's dynamic response, allowing comprehensive testing of the speed control algorithm under a wide range of operating conditions.

Fig. 5. Complex urban scenarios in Morocco used for the evaluation of speed limit sign detection.

Model training was conducted on a high-performance local machine equipped with an AMD Ryzen 9 7940HX CPU, NVIDIA RTX 4070 GPU with 8 GB VRAM, and 32 GB of DDR5 RAM, running Windows 11. The training environment included Python 3.12.4, PyTorch 2.5.1, and CUDA 11.8. The model was trained over 300 epochs with a batch size of 16 using the Stochastic Gradient Descent (SGD) optimizer, configured with a learning rate of 0.01, momentum of 0.937, and weight decay of 0.0005, as summarized in Table II.

TABLE II. MACHINE PARAMETERS

Parameters	Values
Stator resistance R	$R = 2.875\ \Omega$
Direct axis inductance Ld	$Ld = 7.5$ mH
Quadrature axis inductance Lq	$Lq = 2.5$ mH
Moment of inertia J	J = 0.0008 kg.m^2
Coefficient of friction f	$f = 0.0001$ N.m. s
Number of magnetic poles P	$P = 8$

TABLE III. HARDWARE AND SOFTWARE CONFIGURATIONS WITH HYPERPARAMETER SETTINGS

Hardware and software Environment		**Hyperparameters**	
Name	***Version***	***Parameters***	***Details***
CPU	AMD Ryzen 97940HX	Epochs	300
GPU	NVIDIA GeForce RTX4070	Batch size	16
VRAM	8 GB	Image size	640x640
Memory	32 GB DDR5	Optimizer algorithm	SGD
Operating System	Windows 11	Momentum	0.937
Python Version	3.12.4	Weight Decay	0.0005
PyTorch Version	2.5.1	Initial Learning Rate	0.01
CUDA Version	11.8	Final Learning Rate	0.01

III. RESULTS

A. YOLOv11 Traffic Sign Limit Detection

The YOLOv11 model demonstrated exceptional performance during both training and validation phases, achieving highly accurate speed limit sign detection. As shown in Figure 6, the convergence of training and validation losses indicates effective learning and training stability. The model achieved a mAP@50 of 99.6%, reflecting excellent localization accuracy, and a mAP@50-95 of 86.2%, indicating robustness across a range of Intersection over Union (IoU) thresholds. In addition, the model attained a precision of 99.2% and a recall of 98.5%, confirming its ability to minimize false positives while reliably identifying relevant speed limit signs in real-world scenarios. Analysis of the Precision–Confidence curves (Figure 7) shows that precision peaked globally at 1.00 at a confidence threshold of approximately 0.911. Precision remained above 90% across most classes at moderate confidence levels, with particularly strong detection performance for 50 km/h, 70 km/h, and 90 km/h signs. The Recall–Confidence curves (Figure 8) further illustrate YOLOv11's consistent performance, with recall values near 1.0 up to a confidence threshold of approximately 0.8. Beyond this point, recall gradually declines due to stricter filtering, an expected trade-off in high-precision systems. The F1–Confidence curves (Figure 9) highlight YOLOv11's balanced performance, with a global F1-score peaking at 0.99 around a confidence threshold of 0.606. The F1-score remains high across a wide range of thresholds, declining only beyond 0.8, reflecting strong overall detection stability.

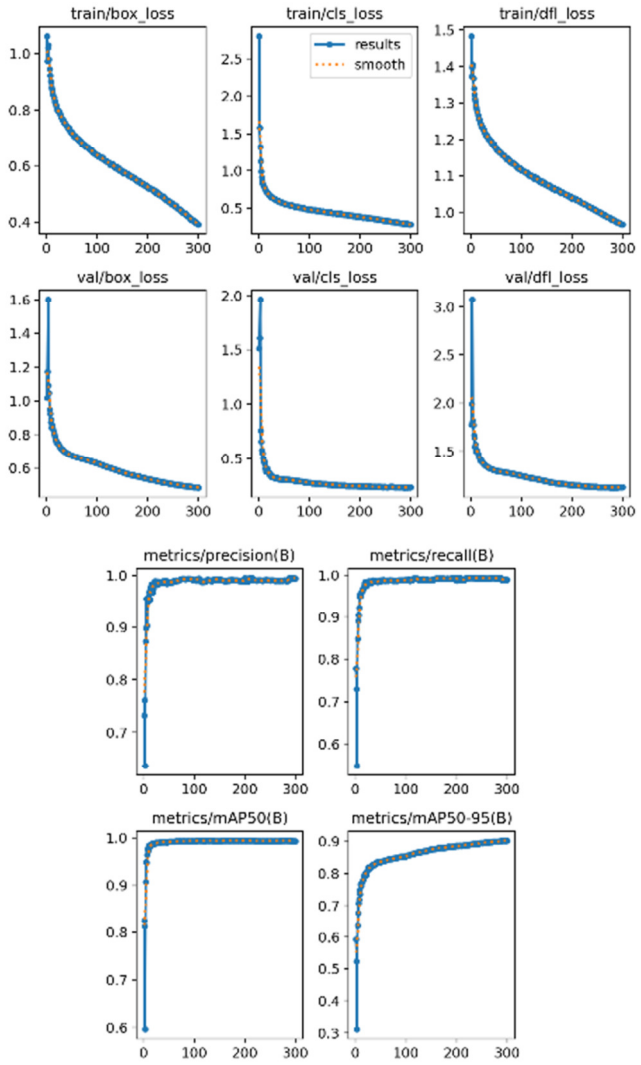

Fig. 6. YOLOv11 training metrics: training losses, validation losses, performance metrics.

The normalized confusion matrix shown in Figure 10 provides a detailed view of classification accuracy across speed limit classes. The matrix displays a heavily populated diagonal, indicating high rates of correct classification. Most classes, including 90 km/h, 100 km/h, and 120 km/h, achieved near-perfect accuracy. Minor misclassifications were observed primarily in the background class, typically due to partially obscured or visually ambiguous signs.

Real-world robustness was further validated in Figure 11, where YOLOv11 effectively detected speed limit signs (30 km/h, 40 km/h, and 60 km/h) despite partial occlusions from tree branches and challenging lighting. This confirms the model's resilience and effectiveness in varied environments, reinforcing its suitability for ADAS and speed regulation in EVs. Table III presents a comparative analysis of YOLOv11 performance with results from previous YOLO versions in the literature for speed limit sign detection. While YOLOv9 achieved a mAP@50 of 98.8% and a mAP@50:95 of 75%, YOLOv11 outperformed it with values of 99.6% and 86.2%, respectively. These improvements stem from architectural refinements, enhanced feature extraction, a more optimized detection pipeline, and the elimination of Non-Maximum Suppression (NMS), which collectively contribute to increased detection accuracy and reliability.

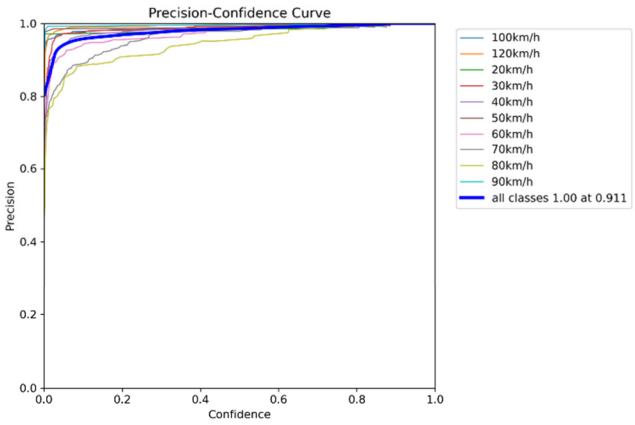

Fig. 7. Precision-confidence curves for each detected speed limit class.

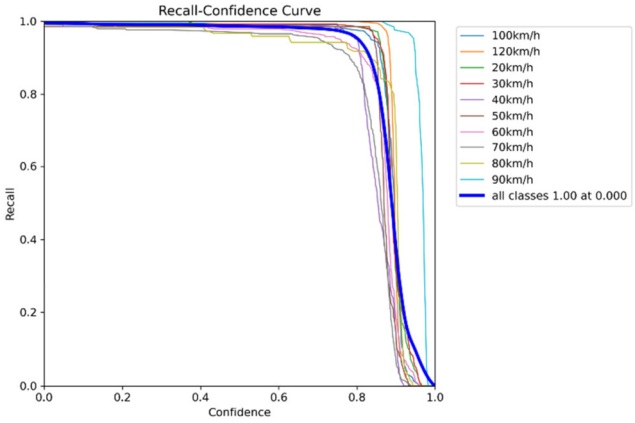

Fig. 8. Recall-confidence performance across speed limit classes.

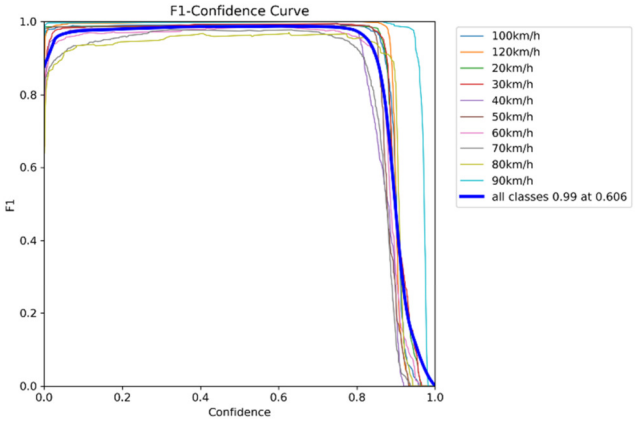

Fig. 9. F1-confidence analysis for YOLOv11 model.

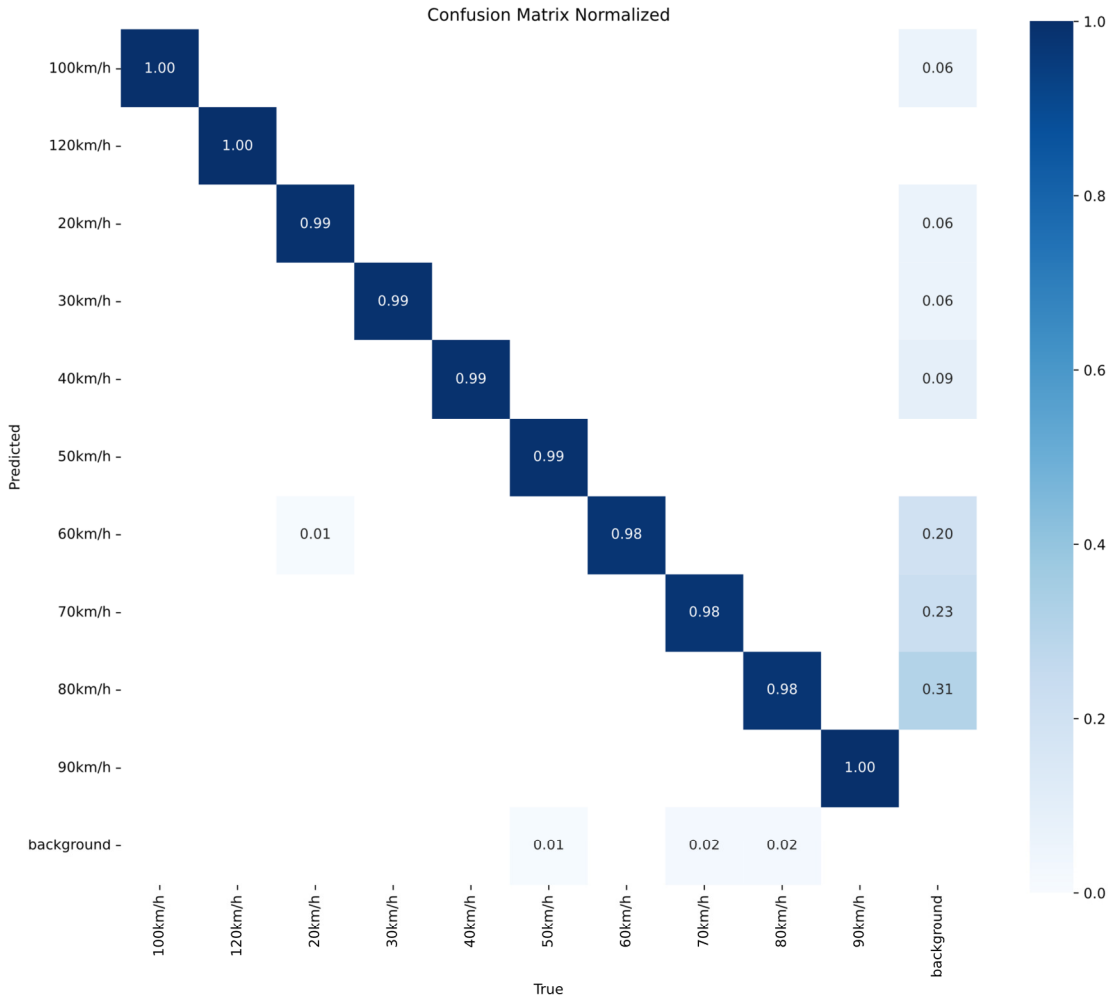

Fig. 10. Normalized confusion matrix for YOLOv11.

Fig. 11. Detection of speed limit signs at different speed levels.

TABLE IV. COMPARISON OF MODELS

Method	Precision (%)	Recall (%)	F1-score (%)	mAP@50	mAP50@95
YOLOv4 [17]	74	81	77	74.6%	-
YOLOv5 [18]	85	82.8	83.9	87.8%	67.2%
YOLOv7 [19]	91.46	83	87	91.4%	-
YOLOv8 [20]	96.1	94.7	95.4	95.3%	-
YOLOv9 [21]	81.29	88.2	89.8	98.8%	75%
YOLOv11	99.2	98.5	98.9	99.6%	86.2%

B. Speed Regulation

Figure 12 presents a simulation of the proposed speed regulation system, which integrates PMSM control with real-time traffic sign detection.

In the first simulation scenario in Figure 12(a), the initial motor speed was set to V_m=77 km/h, while the detected speed limit was 60 km/h. The objective here was to verify the system's capability to significantly decelerate the vehicle to match the required speed limit. Results confirmed that the

speed regulation effectively reduced the motor speed to closely match the imposed speed limit, demonstrating the system's compliance capability. In the second scenario in Figure 12(b), the motor initially operated at V_m = 65 km/h, with a new detected speed limit of 40 km/h. The system quickly adapted, demonstrating rapid convergence of motor speed to the required limit, thus validating its responsiveness and robustness to frequent speed variations. For the third scenario in Figure 12(c), the motor started at V_m = 50 km/h, and the observed speed limit was 30 km/h. The results show proportional and accurate speed reduction, maintaining compliance even when the new speed limit is substantially lower than the initial speed.

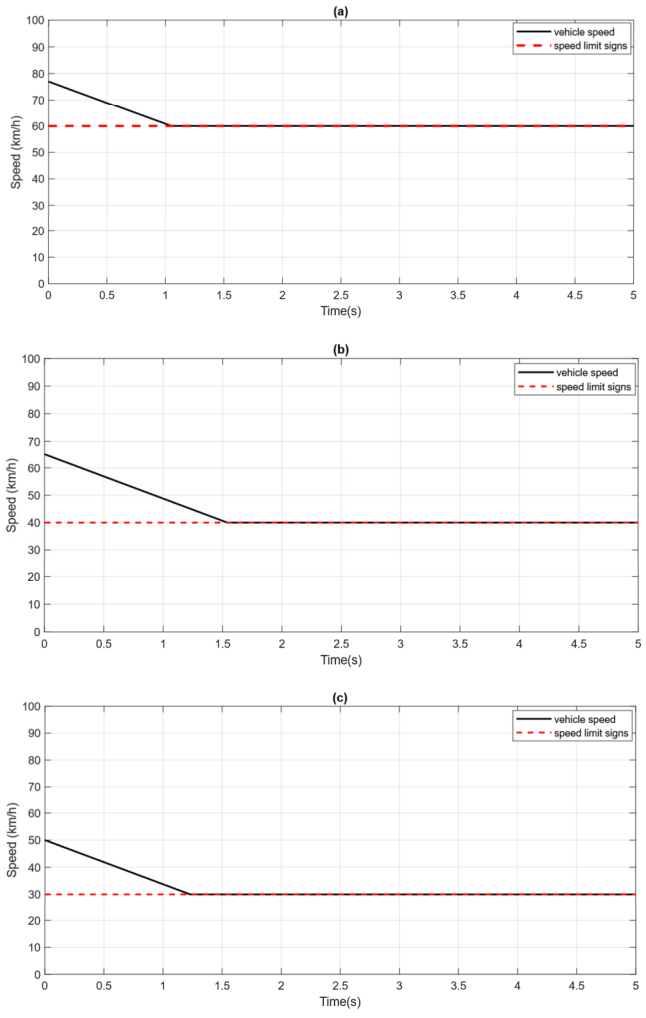

Fig. 12. Vehicle speed regulation under different speed limit scenarios: (a) 60 km/h, (b) 40 km/h, and (c) 30 km/h.

In addition to the proposed vector control strategy for the PMSM system, several alternatives have been explored in the literature. Fuzzy PID controllers [22] offer enhanced robustness and accuracy compared to conventional PID techniques. SMC, when optimized using Harris Hawks Optimization [23], achieves improved dynamic performance and resilience under varying operational conditions. Furthermore, Fuzzy Logic Controllers (FLCs) [24] demonstrate superior torque stability and energy efficiency. Despite these advancements, vector control remains the most appropriate choice for ADAS applications, offering an optimal trade-off between control precision, computational complexity, and real-time implementation feasibility.

IV. CONCLUSION

This study presents a deep learning-based system that integrates YOLOv11 for real-time speed limit sign detection with Permanent Magnet Synchronous Motors (PMSM) vector control for automated vehicle speed adaptation in Electric Vehicles (EVs). The YOLOv11 model, enhanced with C3k2, Spatial Pyramid Pooling Fast (SPPF), and Cross-Scale Pixel Spatial Attention (C2PSA) modules, achieved outstanding detection accuracy, with a mean Average Precision (mAP) of 99.6% (mAP@50) and 86.2% (mAP@50–95), 99% precision, and 98.3% recall, outperforming previous versions of You Only Look Once (YOLO).

In terms of control, the PMSM speed regulation system showed rapid and precise responses under varying speed limit scenarios. While alternative control strategies such as Fuzzy PID, Sliding Mode Control (SMC), and Fuzzy Logic Controllers (FLCs) have demonstrated good accuracy, stability, and efficiency, they often involve increased computational complexity or require extensive tuning. In contrast, vector control offers a superior trade-off between implementation simplicity, real-time adaptability, and reliable performance.

By unifying high-performance traffic sign detection with intelligent motor control, this work significantly advances Advanced Driver Assistance Systems (ADAS) capabilities in EVs. The proposed system enhances road safety and promotes energy-efficient driving through real-time enforcement of speed limits.

REFERENCES

[1] S. Waykole, N. Shiwakoti, and P. Stasinopoulos, "Review on Lane Detection and Tracking Algorithms of Advanced Driver Assistance System," *Sustainability*, vol. 13, no. 20, Oct. 2021, Art. no. 11417, https://doi.org/10.3390/su132011417.

[2] A. A. Mehta *et al.*, "Securing the Future: A Comprehensive Review of Security Challenges and Solutions in Advanced Driver Assistance Systems," *IEEE Access*, vol. 12, pp. 643–678, 2024, https://doi.org/10.1109/ACCESS.2023.3347200.

[3] Y. Li, A. Mogelmose, and M. M. Trivedi, "Pushing the 'Speed Limit': High-Accuracy US Traffic Sign Recognition With Convolutional Neural Networks," *IEEE Transactions on Intelligent Vehicles*, vol. 1, no. 2, pp. 167–176, Jun. 2016, https://doi.org/10.1109/TIV.2016.2615523.

[4] Q. Zhao, Z. Zhao, Z. Yang, and W. Liu, "Speed control of sensorless PMSM drive based on EKF optimized by variable scale chaotic particle swarm optimization," *Measurement and Control*, vol. 57, no. 7, pp. 981–991, Jul. 2024, https://doi.org/10.1177/00202940231224220.

[5] F. Sultana, A. Sufian, and P. Dutta, "A Review of Object Detection Models Based on Convolutional Neural Network," in *Intelligent Computing: Image Processing Based Applications*, vol. 1157, J. K. Mandal and S. Banerjee, Eds. Singapore: Springer Singapore, 2020, pp. 1–16.

[6] J. Redmon, S. Divvala, R. Girshick, and A. Farhadi, "You Only Look Once: Unified, Real-Time Object Detection," in *2016 IEEE Conference on Computer Vision and Pattern Recognition (CVPR)*, Las Vegas, NV, USA, Jun. 2016, pp. 779–788, https://doi.org/10.1109/CVPR.2016.91.

[7] D. Reis, J. Kupec, J. Hong, and A. Daoudi, "Real-Time Flying Object Detection with YOLOv8," May 2024, https://doi.org/10.48550/arXiv.2305.09972.

[8] M. Chaman, A. El Maliki, H. El Yanboiy, H. Dahou, H. Laâmari, and A. Hadjoudja, "Comparative Analysis of Deep Neural Networks YOLOv11 and YOLOv12 for Real-Time Vehicle Detection in Autonomous Vehicles," *International Journal of Transport Development and Integration*, vol. 9, no. 1, pp. 39–48, Mar. 2025, https://doi.org/10.18280/ijtdi.090104.

[9] Ultralytics, *YOLO11*, 2024. [Online]. Available: https://docs.ultralytics.com/models/yolo11

[10] J. Zhao, X. Liu, S. Wang, and L. Zheng, "Review of Design and Control Optimization of Axial Flux PMSM in Renewable-energy Applications," *Chinese Journal of Mechanical Engineering*, vol. 36, no. 1, Apr. 2023, Art. no. 45, https://doi.org/10.1186/s10033-023-00868-8.

[11] F. M. Zaihidee, S. Mekhilef, and M. Mubin, "Robust Speed Control of PMSM Using Sliding Mode Control (SMC)—A Review," *Energies*, vol. 12, no. 9, May 2019, Art. no. 1669, https://doi.org/10.3390/en12091669.

[12] K. Belda and D. Vosmik, "Explicit Generalized Predictive Control of Speed and Position of PMSM Drives," *IEEE Transactions on Industrial Electronics*, vol. 63, no. 6, pp. 3889–3896, Jun. 2016, https://doi.org/10.1109/TIE.2016.2515061.

[13] E. Sangeetha and V. P. Ramachandran, "An enhanced proportional resonance controller design for the PMSM based electric vehicle drive system," *Heliyon*, vol. 10, no. 15, Aug. 2024, Art. no. e35244, https://doi.org/10.1016/j.heliyon.2024.e35244.

[14] A. Awad and S. A. Aly, "Early Diagnosis of Acute Lymphoblastic Leukemia Using YOLOv8 and YOLOv11 Deep Learning Models." arXiv, 2024, https://doi.org/10.48550/ARXIV.2410.10701.

[15] A. Tripathi, V. Gohokar, and R. Kute, "Comparative Analysis of YOLOv8 and YOLOv9 Models for Real-Time Plant Disease Detection in Hydroponics," *Engineering, Technology & Applied Science Research*, vol. 14, no. 5, pp. 17269–17275, Oct. 2024, https://doi.org/10.48084/etasr.8301.

[16] T.-L. Le, "A Robust Control Strategy for Effective Field-Oriented Control of PMSMs," *Engineering, Technology & Applied Science Research*, vol. 14, no. 6, pp. 18469–18475, Dec. 2024, https://doi.org/10.48084/etasr.8893.

[17] A. Mulyanto, R. I. Borman, P. Prasetyawan, W. Jatmiko, P. Mursanto, and A. Sinaga, "Indonesian Traffic Sign Recognition For Advanced Driver Assistent (ADAS) Using YOLOv4," in *2020 3rd International Seminar on Research of Information Technology and Intelligent Systems (ISRITI)*, Yogyakarta, Indonesia, Dec. 2020, pp. 520–524, https://doi.org/10.1109/ISRITI51436.2020.9315368.

[18] L. Jiang, H. Liu, H. Zhu, and G. Zhang, "Improved YOLO v5 with balanced feature pyramid and attention module for traffic sign detection," *MATEC Web of Conferences*, vol. 355, 2022, Art. no. 03023, https://doi.org/10.1051/matecconf/202235503023.

[19] J. P. Q. Tomas, J. C. S. Diamante, M. M. T. Cortez, and G. A. I. Domingo, "Detection of Water Hyacinth (Eichhornia crassipes) on the Water Surface of Pasig River, Philippines, through YOLOv7," in *Proceedings of the 2023 6th International Conference on Computational Intelligence and Intelligent Systems*, Tokyo Japan, Nov. 2023, pp. 124–129, https://doi.org/10.1145/3638209.3638228.

[20] B. Dang Hai, H. D. Nguyen, T. N. Vo, P.-N. Tran, C. T. Nguyen, and D. N. M. Dang, "Performance Comparison in Traffic Sign Recognition Using Deep Learning," in *Industrial Networks and Intelligent Systems*, Da Nang, Vietnam, Feb. 2024, vol. 595, pp. 122–138, https://doi.org/10.1007/978-3-031-67357-3_9.

[21] S. Fang, C. Chen, Z. Li, M. Zhou, and R. Wei, "YOLO-ADual: A Lightweight Traffic Sign Detection Model for a Mobile Driving System," *World Electric Vehicle Journal*, vol. 15, no. 7, Jul. 2024, Art. no. 323, https://doi.org/10.3390/wevj15070323.

[22] F. Jin, H. Wan, Z. Huang, and M. Gu, "PMSM Vector Control Based on Fuzzy PID Controller," *Journal of Physics: Conference Series*, vol. 1617, no. 1, Aug. 2020, Art. no. 012016, https://doi.org/10.1088/1742-6596/1617/1/012016.

[23] K. Mathew K, D. M. Abraham, and A. Harish, "Speed regulation of PMSM drive in electric vehicle applications with sliding mode controller based on harris Hawks optimization," *e-Prime - Advances in Electrical Engineering, Electronics and Energy*, vol. 9, Sep. 2024, Art. no. 100643, https://doi.org/10.1016/j.prime.2024.100643.

[24] R. Shenbagalakshmi, S. K. Mittal, J. Subramaniyan, V. Vengatesan, D. Manikandan, and K. Ramaswamy, "Adaptive speed control of BLDC motors for enhanced electric vehicle performance using fuzzy logic," *Scientific Reports*, vol. 15, no. 1, Art. no. 12579, Apr. 2025, https://doi.org/10.1038/s41598-025-90957-6.